Supramolecular Chemistry

Cyclodextrin 'Chaperones' Enable Quasi-Ideal Supramolecular Network Formation and Enhanced Photodimerization of Hydrophobic, Red-shifted Photoswitches in Water

Daniel Hoenders, Simon Ludwanowski, Christopher Barner-Kowollik,* and Andreas Walther*

Abstract: Precision-engineered light-triggered hydrogels are important for a diversity of applications. However, fields such as biomaterials require wavelength outside the harsh UV regime to prevent photodamage, typically requiring chromophores with extended π-conjugation that suffer from poor water solubility. Herein, we demonstrate how cyclodextrins can be used as auxiliary agents to not only solubilize such chromophores, but even to preorganize them in a 2:2 host-guest inclusion complex to facilitate photodimerization. We apply our concept to styrylpyrene-end-functionalized star-shaped polyethylene glycols (sPEGs). We initially unravel details of the host-guest inclusion complex using spectroscopy and mass spectrometry to give clear evidence of a 2:2 complex formation. Subsequently, we show that the resultant supramolecularly linked hydrogels conform to theories of supramolecular quasi-ideal model networks, and derive details on their association dynamics using in-depth rheological measurements and kinetic models. By comparing sPEGs of different arm length, we further elucidate the model network topology and the accessible mechanical property space. The photo-mediated dimerization proceeds smoothly, allowing to transform the supramolecular model networks into covalent ones. We submit that our strategy opens avenues for executing hydrophobic photochemistry in aqueous environments with enhanced control over reactivity, hydrogel topology or programmable mechanical properties.

Introduction

Photochemistry is a powerful tool to control soft materials and to enable applications requiring spatiotemporal and remote control in materials and life science.[1] For very advanced photochemistries, light-triggered reactions can even be wavelength-selective.[2] Amongst such photochemical reactions, photo-induced cycloadditions, i.e., [2+2] and

[*] Dr. D. Hoenders, Dr. S. Ludwanowski, Prof. Dr. A. Walther
Life-Like Materials and Systems Lab, Department of Chemistry,
University of Mainz
Duesbergweg 10–14, 55128 Mainz, Germany
E-mail: andreas.walther@uni-mainz.de

Prof. Dr. C. Barner-Kowollik
School of Chemistry and Physics and Centre for Materials Science,
Queensland University of Technology (QUT),
2 George Street, 4000 Brisbane, QLD, Australia
E-mail: christopher.barnerkowollik@qut.edu.au

Prof. Dr. C. Barner-Kowollik
Institute of Nanotechnology (INT),
Karlsruhe Institute of Technology (KIT),
Hermann-von-Helmholtz-Platz 1,
76344 Eggenstein-Leopoldshafen, Germany
E-mail: christopher.barner-kowollik@kit.edu

[4+4] cycloaddition, are highly attractive for biological applications as they proceed under mild conditions and do not require additives such as photo-initiators or catalysts. Photo-induced covalent polymer network formation for hydrogel fabrication in water has been mostly shown for anthracene,[3] coumarin,[4] cinnamate,[5] and stilbene.[6] However, these compounds require short-wavelength UV light, which may make them challenging for use in biological media and in the presence of living cells, although a recent study has demonstrated that mild-UV can indeed constitute a wavelength regime for biological studies.[7] In terms of photochemical network formation under biologically benign conditions, one option includes radical-based crosslinking approaches, which amplify the quantum yield of initiation processes dramatically, thus requiring minimal light input, yet introduce highly reactive free-radical species. In the realm of non-quantum efficiency amplified systems, the focus has shifted to the development of chromophores that can undergo cycloaddition with visible light of wavelengths well above 400 nm.[8] This red-shift in light activation limits the photodamage to synthetic and biological matter, increases the penetration depth, and allows λ-orthogonality by combination of different chromophores.[9] However, modification of the chromophores to become activatable by light of the red-shifted spectrum comes at the expense of larger conjugated systems, even though push-pull electronic substituents around chromophores can limit the size of the chromophore to some extent. Significantly red-shifted molecules oftentimes become poorly soluble in aqueous media,

which restricts their application in designing defined systems or when targeting higher concentrations of photoactive units —a critical aspect when designing hydrogels.

One classical way to solubilize hydrophobic compounds in water is the use of host-guest inclusion complexation. In such systems, a suitable water-soluble cavitand can host and solubilize non-polar compounds such as a chromophore as a guest within its cavity well beyond classical solubility limitations in plain solution. Some of the most common hosts in water are cyclodextrins (CD) and cucurbiturils (CB). Such host-guest chemistries have already been used in combination with photoactive compounds, including in the realm of responsive and adaptable materials design.[10] Most prominently, the ability of photoswitches to change their propensity to be included in CD cavities under light irradiation has opened a wide array of applications. Their light-induced polarity change enables debonding on-demand, which has been exploited, for example, in the construction of light-adaptable micelles, vesicles, gels and surfaces.[9] Perhaps the most exploited photoswitches in this context are azobenzene derivatives, yet photofragmentation systems based on *ortho*-nitrobenzaldenhydes have also been exploited, with some systems making use of [2+2] pericyclic reactions. γ-cyclodextrin (γ-CD) has even been applied for supramolecular photochirogenesis, i.e., engineering photochemical selectivity in [2+2] cycloadditions of small chromophores, such as anthracene derivates. An excellent overview on the most prominent systems can been found in literature.[10i] On a general macroscopic level, host-guest interactions themselves can serve to design tunable materials based on dynamic supramolecular crosslinks.[11] However, it has thus far been unclear whether these approaches may also be beneficial for comparably large, red-shifted photodimerization units that take up considerably more volume than classically used anthracene or coumarin, with a view to making them a viable option for network construction using mild visible light wavelengths. Herein, we close this critical gap.

Herein, we develop and characterize a new photosensitive supramolecule derived from styrylpyrene (StyP) and γ-CD. StyP belongs to the class of red-shifted [2+2] photodimerization compounds[8c] that suffer from a large hydrophobic body with poor solubility. We investigate the host-guest complex formation in water for a small model compound and demonstrate that γ-CD does not only enhance the otherwise restricted solubility of StyP in water, but also accelerates the photodimerization process. Furthermore, we use multi-armed star-shaped polymers (sPEGs; PEG=polyethylene glycol) containing StyP as end groups to study the behavior of the complex in aqueous media and find that it forms reversible supramolecular hydrogel networks with ideal Maxwell behavior. By analyzing the temperature-dependent characteristics of the network, we derive the kinetics and thermodynamics of the complex and design dynamic hydrogel networks that can be converted into static networks through photodimerization.

Results and Discussion

Basic Material Concept

Our basic material concept addressing the challenge to use red-shifted hydrophobic photoswitches with extended π-frameworks for the formation of hydrogels with the assistance of host-guest inclusion complexes is depicted in Scheme 1. We hypothesize that a water-soluble host, cyclodextrin, overcomes solubility limitations and potentially allows for aggregation- and defect-free network formation. As photoreactive chromophore, we selected styrylpyrene, which is a well-known photoreactive entity undergoing a photo-induced dimerization at ca. 435 nm.[8c] The dimerization can be reversed at lower wavelength, which is however not core of the current study. Due to the large aromatic framework, we envisaged that γ-CD would be most suitable for an efficient host-guest complex formation,[12] even with the possibility for a 2:2 complex formation that would enable to accelerate the photodimerization due to spatial proximity effects. To construct hydrogels, we selected star-shaped PEG of different arm number and length and tethered the StyP to the end of each arm to generate multifunctional prepolymers. An early glimpse into the benefits of the strategy is provided in Scheme 1, where the photographs show phase separation of a 4-arm sPEG-StyP (20 kDa, 7 wt %) with near complete StyP functionalization in the absence of γ-CD, whereas the presence of γ-CD (equimolar to StyP) leads to a homogeneous solution.

Synthesis of the Materials

Table 1 gives an overview of the synthesized 4-arm and 8-arm sPEG-StyPs with total number average molecular weights, M_n, of 20 and 40 kDa. To attach the StyP end group, we performed a DMTMM (4-(4,6-dimethoxy-1,3,5-triazin-2-yl)-4-methyl-morph-olinium)-mediated amide formation between amine-terminated sPEGs and a carboxylate-functionalized StyP derivative (Figure S1a). The degree of functionalization (by ^{1}H-NMR) is well above 90 %; in most cases near quantitative (Table 1).
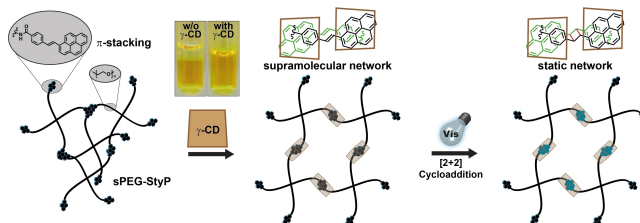
Scheme 1. Concept for supramolecular-assisted predefined network formation, able to be locked on demand upon irradiation with blue light. We note that the idealized depiction of a "perfect" network is oversimplified, and some remaining dangling chains or unproductive loops may form. Their content is, however, minimized when working at the overlap concentration.[13]

Table 1: Overview of sPEG-StyP library.

Starting material	Arm length (DP_n)[a]	Overlap concentration c* (wt%)[b]	Degree of functionalization (%)[c]
Linear TOTA[d]	3	–	100
4-arm sPEG 20 kDa	112	7	98
4-arm sPEG 40 kDa	230	4	90
8-arm sPEG 20 kDa	55	13	96
8-arm sPEG 40 kDa	105	7	96

[a] Based on data from manufacturer. [b] Based on rheology measurements with sPEG-OHs of similar size. [c] As determined from NMR. [d] Linear reference compound.

For model studies regarding the complex formation, we also prepared a linear methyl-EO$_3$-based derivative (TOTA = 4,7,10-trioxa-13-tridecanamine). We further determined the overlap concentrations of the individual sPEGs using rheology (Figure S6). Notably, the overlap concentration of 4-arm sPEG (20 kDa) and 8-arm sPEG (40 kDa) are identical, meaning that the concentrations of crosslinks per volume element is identical. Overall, the well-defined nature of the sPEGs enables the quantitative characterization of the resultant properties on the hydrogel level.

Study of the Inclusion Complex Using Model Compounds

We initially conducted in-depth investigations on the supramolecular chemistry of the StyP/γ-CD host-guest inclusion complex on the molecular level using the reference compound TOTA-StyP via extensive NMR and UV/Vis spectroscopy, as well as mass spectrometry. UV/Vis absorption measurements of TOTA-StyP/γ-CD ([G]/[H]; G = TOTA-StyP, H = γ-CD) mixtures at different [G]/[H] ratios show a steep change at a characteristic absorption band of StyP (431 nm) up to a molar ratio of TOTA-StyP/γ-CD = 1:1 (Figure S2a, b). A plateau occurs upon further increasing the γ-CD. This is indicative of an interaction and of a 1:1 interaction.

Further, ^{1}H NMR spectra at different [G]/[H] ratio show that only at a 1:1 ratio all broad aromatic resonances of the poorly soluble TOTA-StyP are shifted (see e.g. 2.94, 3.28, 6.55 and 7.20 ppm; Figure 1a). Concurrently, the major γ-CD resonances in the region of 3.80–4.00 disappear as well. New resonances appear at 3.40–3.80 ppm, confirming the intimate complex formation. Excess of any of the components results in additional resonances from the pristine substances not contributing to the complex formation. Thus, these ^{1}H NMR measurements suggest a 1:1 complex formation in terms of molar ratios, with little flexibility for off-stochiometric complexes.

Due to the large cavity size of the γ-CD, it is however unclear whether this 1:1 molar ratio also translates into a 1:1 complex or a 2:2 complex. Clear evidence for a 2:2 complex is provided by mass spectrometry of an equimolar ratio of TOTA-StyP/γ-CD. Figure 1b shows an isotope pattern with a spacing of m/z = 0.5, indicating a +2 charged state consistent with the calculated result of [2TOTA-StyP@2γ-CD+2H]$^{2+}$ (further details in Figure S3). Furthermore, the simulated mass spectrum of C$_{166}$H$_{238}$N$_4$O$_{88}^{2+}$ (2:2
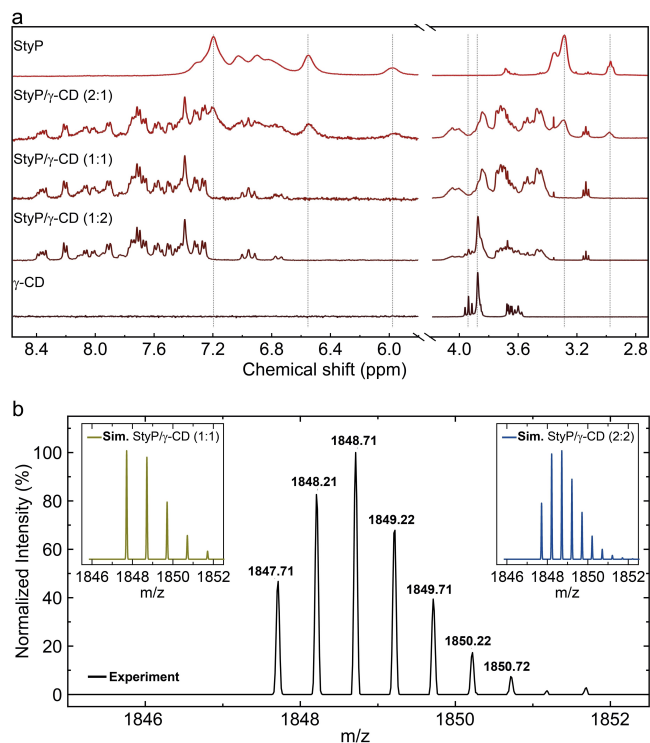

Figure 1. TOTA-StyP/γ-CD forms a 2:2 host-guest complex in water. (a) ^{1}H NMR spectra at different ratios of TOTA-StyP/γ-CD (D$_2$O). The proton resonances of TOTA-StyP (2 mM) are shielded owing to π-π stacking in D$_2$O (top). Off-stochiometric mixtures reveal the presence of pristine compounds. (b) The mass spectrum (pos. mode) of an equimolar ratio of TOTA-StyP/γ-CD (both 0.5 mM) in water shows a strong signal with maximum at $m/z = 1848.71$. The simulated mass spectra of C$_{166}$H$_{238}$N$_4$O$_{88}^{2+}$ (2:2 complex) agrees, whereas a simulated 1:1 complex C$_{83}$H$_{119}$N$_2$O$_{44}^+$ does not. These results confirm the presence of a 2:2 inclusion complex of TOTA-StyP and γ-CD in water.

complex) shows the same isotope pattern at $z = 2$ (inset top right), whereas a 1:1 simulated complex C$_{83}$H$_{119}$N$_2$O$_4^{4+}$ does not fit. Hence, it is a 2:2 host-guest complex.

Additional 2D ^{1}H-NOESY NMR (detailed discussion in Figures S4–S5) indicates that the 2:2 complex is a mixture of three major types of 2:2 host-guest inclusion isomers, wherein the StyPs are arranged in a stacked anti-parallel fashion, whereas the γ-CD are arranged with their larger or smaller openings in the direction of the polymer chain.

Accelerated Photodimerization Assisted by γ-CD

To investigate the feasibility of photodimerization inside the inclusion complex, we performed in situ spectroscopic analysis during the photo-dimerization of TOTA-StyP (48 μM) at 430 nm (Figure 2).[8c] Both time-dependent UV/Vis plots in the absence and presence of γ-CD display a decrease of the absorbance at 381 nm and a concurrent increase of a new peak at 340 nm. Slight differences exist from 350 to 300 nm as the StyP spectrum is influenced by the γ-CD (Figure S2a).

Critically, a quantification of the kinetics, by monitoring the decrease at 381 nm, clearly shows a significantly accelerated reaction when γ-CD is present (blue, StyP/γ-CD; Figure 2c) as compared to when γ-CD is absent (grey, StyP; Figure 2c). The dimerization not only proceeds faster but also to higher conversion in the presence of γ-CD, as two StyP molecules are in close proximity within the cavity of two γ-CDs in the proposed 2:2 complex formation. Thus, the presence of γ-CD is not only beneficial for the overall solubility of larger polymers (Scheme 1), but also for the reactivity of the photoswitch.
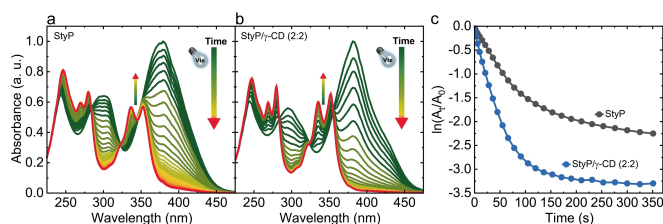

Figure 2. γ-CD accelerated photodimerization of TOTA-StyP. Time-resolved UV/Vis of the blue light induced dimerization of TOTA-StyP (48 μM) in water in either (a) absence or (b) presence of γ-CD (48 μM; $\lambda = 430$ nm, 20 mW cm^{-2}, 6 min). (c) The first-order kinetic plots for (a) and (b) at 381 nm show accelerated and more quantitative dimerization in presence of γ-CD.
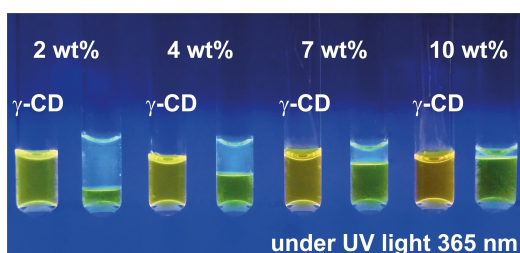

Figure 3. γ-CD is a solubilizer and gelator for sPEG-StyP. Solubility enhancement of 4-arm sPEG-StyP 20 kDa (2–10 wt%) with and without equimolar quantities of γ-CD compared to the StyP end groups. Photographs under UV light. γ-CD leads to a complete dissolution of sPEG-StyP and supramolecular network formation. In absence of γ-CD the polymer only swells in water leading to macroscopic phase segregation.

Characterization of Supramolecularly Linked Networks

Since the above investigations confirmed a 2:2 complex, we expected the formation of supramolecular dynamic networks that we characterized before turning to photo-crosslinking. For a simple macroscopic test, we initially added 4-arm sPEG-StyP 20 kDa to pure water at four different concentrations below and above the overlap concentration of 7 wt% in absence or presence of equimolar concentrations of γ-CD (compared to StyP). Critically, the photographs taken under UV light demonstrate that the hydrophobically modified sPEG-StyP does in fact only swell in plain water (right hand vials with water supernatant phase, Figure 3), whereas the γ-CD assists in the complete dissolution and supramolecular network formation. The assistance of the γ-CD in the dissolution of the StyP segments is also visible in a change in the fluorescence emission from green to yellowish. This change in fluorescence emission can also be observed for model complexes of TOTA-StyP at different concentrations of γ-CD (Figure S2c, d), confirming that the complex formation also operates for the polymeric structures. It underscores the key importance of the γ-CD to act as a solubilizing and pre-ordering chaperone.

For the characterization of the γ-CD-linked supramolecular networks, we performed rheological measurements at the overlap concentrations (c*) of the individual sPEGs. Working at c* allows forming networks with a close to ideal structure as entanglements and loop formation of end groups are minimized,[13–14] opening the possibility for the best comparison of mechanical properties.

Figure 4a displays frequency sweeps for all sPEG-StyPs/γ-CD as a function of the angular frequency, ω, at 20°C. All four systems exhibit similar behavior regarding the development of G' and G'' and show a crossover at $\omega \approx 10$ rad s^{-1}, separating the predominantly elastic behavior at higher frequency from a Maxwell behavior at lower frequency. The associated relaxation time corresponds to the cleavage of the supramolecular host-guest inclusion complexes.[15] Minor differences in the individual relaxation times should not be overinterpreted on the logarithmic axis. At lower frequencies, $G'' \propto \omega$, whereas $G' \propto \omega^2$, which is indicative of near perfect Maxwell behavior and of an ideal reversible polymer network.[14b] At higher frequencies, the network behaves as a covalent network. The most important differences can be seen when comparing the developing G' plateau values at higher frequencies. Note that the plateaus are not fully developed for all samples because the rheometer cannot measure at higher frequencies. Since these covalent-like networks do not undergo bond dynamics, one can infer the density of crosslinks. Clearly, the 4-arm sPEG-StyP 40 kDa with the longest arms leads to the lowest G' value, whereas the 8-arm sPEG-StyP 20 kDa with the shortest arms leads to the highest G' value. The 8-arm sPEG-StyP 40 kDa and the 4 arm sPEG-StyP 20 kDa, having the same arm length, lead to nearly the same G' value, indicating that the stiffness of the materials can be programmed for multifunctional sPEGs predominantly via the arm length at the overlap concentration, whereas the multifunctionality of the core at the same arm length and overlap concentration only plays a
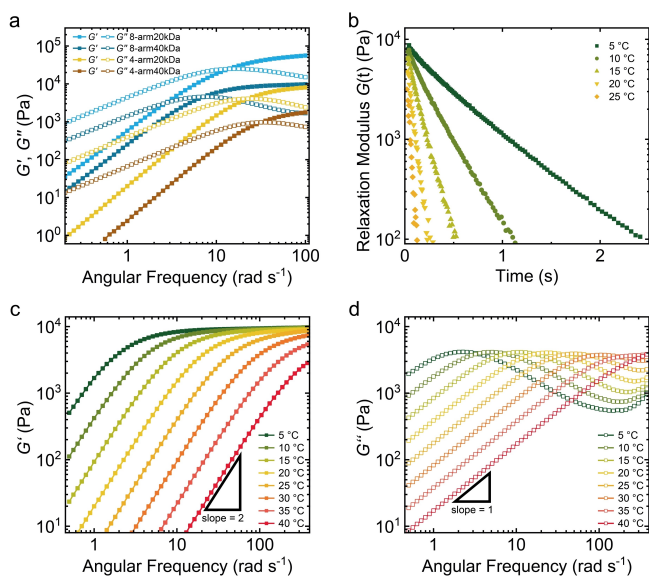
Figure 4. Rheological characterization of sPEG-Styp/γ-CD supramolecular networks. (a) Frequency sweeps of four different sPEG-StyPs at c* in presence of equimolar amounts of γ-CD in relation to StyP (T = 20 °C, amplitude, γ = 1 %, c* in Table 1). The moduli are frequency-dependent with viscous-dominant flow (G' < G'') at low frequency and elastic behavior (G' > G'') at high frequency. (b) Stress relaxation shear moduli show that the system relaxes faster with increasing temperature until it reaches 25 °C (shear strain = 10 %). Relaxation times at higher temperature are too fast to be accurately measured. (c–d) Temperature-dependent frequency sweeps ((c) G' and (d) G'') for 4-arm sPEG-StyP 20 kDa/γ-CD (c* = 7 wt %, c(γ-CD) - = 14 mM, γ = 1 %). The elastic-dominant region (G' > G'') decreases with increasing temperature. Scaling laws apply, $G' \propto \omega^2$ and $G'' \propto \omega$, indicative that the network follows the Maxwell model.

minor role. These observations speak to rather defect-free and highly programmable network properties, as discussed by Sakai and co-workers for covalently linked sPEGs.[14a,16]

To establish a deeper understanding of the influence of the supramolecular bonds and their dynamics on the network properties, we performed additional temperature-dependent frequency sweeps for the 4-arm sPEG-StyP 20 kDa in the range of 5–40 °C (Figure 4c–d), as well as stress relaxation tests (Figure 4b). Both the G' as well as the G'' traces show consistent self-similar shifts as a function of temperature. Clearly, the elastic components become dominant at lower temperature (for example, refer to the more pronounced plateau in G'), whereas viscous dissipation increases at higher temperatures based on the increased exchange dynamics at higher temperature, as the activation energies for formation and dissolution of a complex can be more readily overcome. This can be corroborated by stress relaxation experiments that show vastly enhanced stress relaxation at higher temperatures due to a faster remodeling of a strained network. In summary, our rheological characterization underscores the basic principles of the programmability of the mechanical properties using the γ-CD assisted solubilization, a close to ideal model network formation, and moreover highlights that the complexes remain dynamic (as

a function of temperature) despite their relatively bulky 2:2 complexation.

Since the dynamics of the supramolecular networks are temperature-dependent, it is desirable to gain deeper insights into the kinetic parameters, and in particular the activation energies for association and dissociation. Earlier, Parada and Zhao[14b] developed a quantitative description of such parameters in an ideal reversible network formed by two star polymers bearing complementary functions (A and B) that can undergo complex formation to form C. Since the rheological analysis of our networks (Figure 4) points to a near ideal network with defined rheological characteristics, that is Maxwell behavior, we hypothesized that this model may be transferable to the present sPEG-StyP/γ-CD system, whereby we focus on the 4-arm sPEG-StyP 20 kDa system as a representative example.

The key assumption in applying this model to the present system is to simplify the association behavior of the 2:2 host-guest complex to a situation assuming one star population being only composed of sPEG-StyP (component A) in combination with a second population of sPEG-StyP-CD$_2$ (component B). Even though it is a simplification, we submit that it is not a critical oversimplification, because the important step for changes in the rheological behavior is the association of component A with component B to the rheologically active junction C, or vice-versa their dissociation.

Following the theory by Parada and Zhao, the important input parameters are the instantaneous shear modulus G_0 that can be both obtained from oscillatory rheology as well as stress relaxation measurements (i.e., G' plateau modulus in oscillatory rheology at high frequency, see Figure 4c). Additionally, the relaxation timescale, τ, is needed from both measurements.

Since the network is solely based on the equilibrium concentration of elastically active chains, we can formulate an equilibrium reaction between the forward association rate, k_+, and the backward dissociation rate, k_-, that can be combined in a mass action law.

$$K = \frac{k_+}{k_-} \tag{1}$$

This reflects the equilibrium reaction of:

$$A + B \underset{k_-}{\overset{k_+}{\rightleftharpoons}} C$$
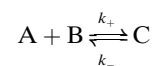
in which C reflects the bound 2:2 complex. A and B are the components introduced above.

The relaxation time τ is commonly associated with the dissociation rate k_- of the reversible crosslink ($k_- = \frac{1}{\tau}$), an assumption that is supported by literature.[14b,15,17] The association rate k_+ can be derived from the equilibrium constant K, that is accessible using the two following equations:

$$\frac{G_0}{k_B T} = \frac{N_A}{16}\left(3 - \sqrt{\frac{4}{p} - 3}\right)^3 \left(\sqrt{\frac{4}{p} - 3} + 1\right) \tag{2}$$

$$p = \left(1 + \frac{1}{2N_A K}\right) - \left[\left(1 + \frac{1}{2N_A K}\right)^2 - 1\right]^{\frac{1}{2}} \tag{3}$$

wherein, N_A is the concentration of functional groups A, p is the conversion of functional groups A as defined by $p = \frac{N_C}{N_A}$ (note that A equals B), G_0 is the instantaneous shear modulus, and K is the equilibrium constant. Importantly, in the calculations of the concentration of A functional groups, the total concentration of polymer needs to be divided into half to account for an equimolar presence of B.

After having obtained K, the k_+ association rate is directly computable using the combination with the k_- dissociation rate (Eq. (1)). Following a linearization of the temperature-dependent rate constants, the activation energies for association, E_{A+}, and dissociation, E_{A-}, are directly accessible from classical Arrhenius behavior (Eq. (4) and Eq. (5)):

$$k_+ = k_0 + \exp\left(\frac{-E_{A+}}{k_B T}\right) \tag{4}$$

$$k_- = k_0 + \exp\left(\frac{-E_{A-}}{k_B T}\right) \tag{5}$$

Figure 5 depicts the corresponding data and the workflow. Common to both data sources, oscillatory rheology and stress relaxation, is the fact that we find a higher activation energy for the dissociation ($E_{A-} = 108\ \text{kJ mol}^{-1}$ for oscillatory rheology and $E_{A-} = 88\ \text{kJ mol}^{-1}$ for stress relaxation) as compared to the one for the association ($E_{A+} = 91\ \text{kJ mol}^{-1}$ for oscillatory rheology and $E_{A+} = 76\ \text{kJ mol}^{-1}$ for stress relaxation). Common to both methods is also an increase in both rate coefficients (Figure 5e) and a decrease in K with temperature (Figure 5b), which is consistent with the general dynamization and softening of the gels at high temperature. These similar trends show a robustness of the overall calculation method.

Due to the very fast relaxation at high temperatures, the stress relaxation measurements lack accuracy. We still prefer to plot some data at $T \geq 25\,°\text{C}$, but do not consider them for the Arrhenius fit. Thus, the classical oscillatory shear rheology is somewhat more robust. Overall, the higher E_{A-} shows that dissociation is hindered compared to association and that the gel formation is thermodynamically and kinetically preferred. The difference in E_A between dissociation and association amounts to ca. 20% for both methods.

Further, transition state theory together with the Eyring equation provide additional insights into the thermodynamic behavior of the supramolecular network (Figure S7).[17b] The determined enthalpy, $\Delta H_{\pm}^{\ddagger}$, and entropy, $\Delta S_{\pm}^{\ddagger}$, for the dissociation activation are $106\ \text{kJ mol}^{-1}$ and $141\ \text{J mol}^{-1}\text{K}^{-1}$, respectively. These results indicate that the process of binding hydrophobic StyP to γ-CD results in an entropic
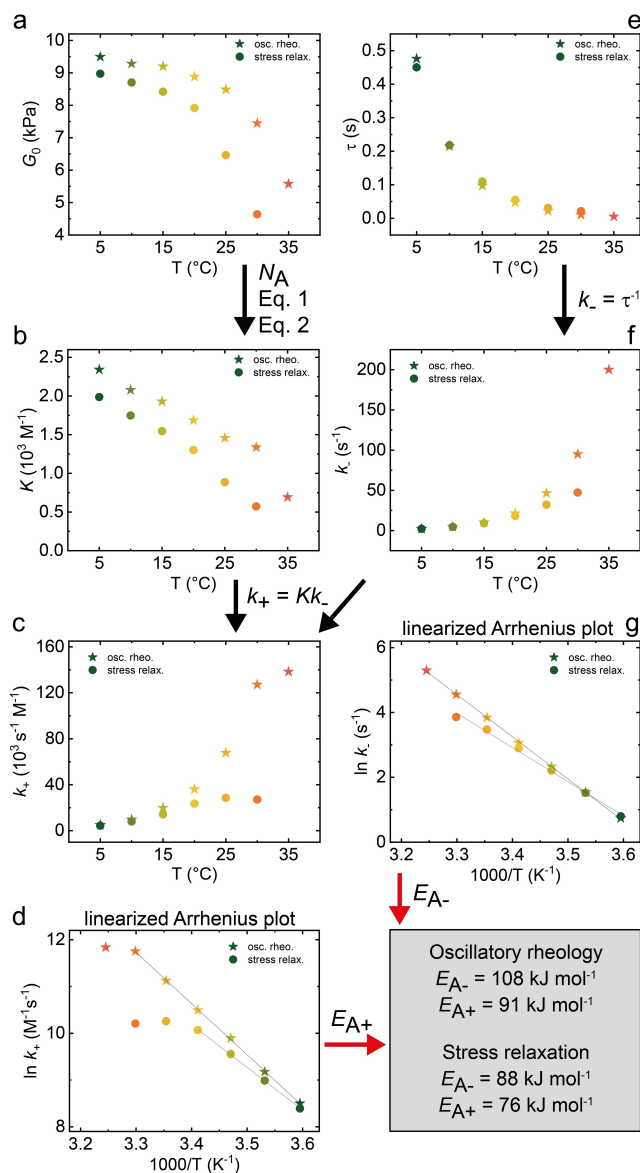

Figure 5. Determination of kinetic parameters of the supramolecular network for 4-arm-StyP 20 kDa (c* = 7 wt%, c(γ-CD) = 14 mM) from rheology and stress relaxation. (a–b) G_0 obtained from the frequency sweeps allow to calculate K. (c) The temperature dependent k_+ parameter can be obtained in combination with the k_- parameter that is derived from the G'/G'' crossover frequency (e–f). (d, g) The linear forms allow to calculate the activation energies for association E_{A+} and dissociation E_{A-} following Arrhenius law.

penalty.[15] The penalty may be due to factors such as the rearrangement of associative StyP stacking or changes in the conformation of the inclusion complex involved in the binding interaction.

In summary, the thorough characterization of the network parameters provides a deep understanding of the kinetics and thermodynamics of even very complex supramolecular gels.

Photo-Crosslinking from Supramolecular Dynamic to Covalent Static Networks

Building on the above derived understanding on having close to ideal model supramolecular networks (Figures 4,5), and the successful and enhanced photodimerization of the StyP units in the model compound TOTA-StyP (Figure 2), we subsequently turn to the photo-crosslinking of the supramolecular networks into permanently linked static hydrogels (Figure 6). Unfortunately, it is not possible to follow the photo-crosslinking of the hydrogels spectroscopically due to a too high optical density of chromophores (further related discussion refer to Figure S8). Therefore, we turn directly to rheology on a rheometer equipped with a glass plate, and report time-dependent measurements during constant irradiation at 430 nm at an angular frequency of $1 \, \text{rad} \, \text{s}^{-1}$, hence in the dynamic regime dominated by viscous dissipation (Figure 4a).

All four sPEG-StyP/γ-CD systems display clear transitions from a visco-elastic liquid with $G'' > G'$ to an elastic solid with $G' > G''$ within 5 min of irradiation (Figure 6a,b,d,e; irradiation starts at 10 min). A plateau is reached for G'' and G' in all systems after ca. 20 min, confirming a very efficient photo-crosslinking process within the model supramolecular network. Interesting dependencies can be derived when quantifying the relevant parameters. Like the above, the softest and stiffest gels are formed by 4-arm sPEG-StyP 40 kDa and 8-arm sPEG-StyP 20 kDa, respectively. The plateau G' values span a wide range from 3 kPa to 125 kPa. Similarly, the sPEGs with similar arm length, i.e., 4-arm sPEG-StyP 20 kDa and 8-arm sPEG-StyP 40 kDa, again lead to similar plateau values of ca. 12.5 kPa, again reflecting that rather the arm length and not the multifunctionality of the core dominate the mechanical properties. It may also be noted that similar correlations are found for the starting G' value and the G'/G'' crossover (Figure 6f), confirming that the supramolecularly preorganized networks can be smoothly transferred into covalent and static networks. Crosslinked systems show significantly less frequency-dependent behavior with $G' > G''$ over 2.5 decades in frequency (Figure 6c). Although decrosslinking by irradiating with an appropriate wavelength (340 nm) is not within the scope of the current study, a simple experiment with a 340 nm light source of $5 \, \text{mW} \, \text{cm}^{-2}$ did not lead to dissolution. Such an observation is in line with earlier findings by Truong et al., who demonstrated an only 7.5 % loss in G' after irradiating a 8 wt % gel (comparable) with a much higher intensity of $20 \, \text{mW} \, \text{cm}^{-2}$.[8b]

In a final step to underscore the versatility of the approach, we raised the question to what extent such a supramolecular chemistry and even photo-crosslinking are applicable in the bulk state, where photodimerizations are kinetically challenged due to slow polymer relaxation and diffusion dynamics. In short, it is indeed possible to transfer the predefined StyP/γ-CD networks into a solvent-free bulk state, and the supramolecular host-guest inclusion complexation helps the kinetics of the photoconjugation. However, due to the presence of the bulky γ-CD, the material properties are intrinsically more affected in the bulk state compared to the hydrogel state, complicating an in-depth analysis. The dynamics of the host-guest inclusion complex are lost in bulk, and photodimerization only weakly contributes to additional mechanical strengthening of an already very non-dynamic, almost covalent host-guest bond. Most pronounced differences appear regarding temperature stability of the mechanical properties after photo-crosslinking. A detailed discussion can be found in part 2.6, Scheme S1 and Figure S9 in the Supporting Information.
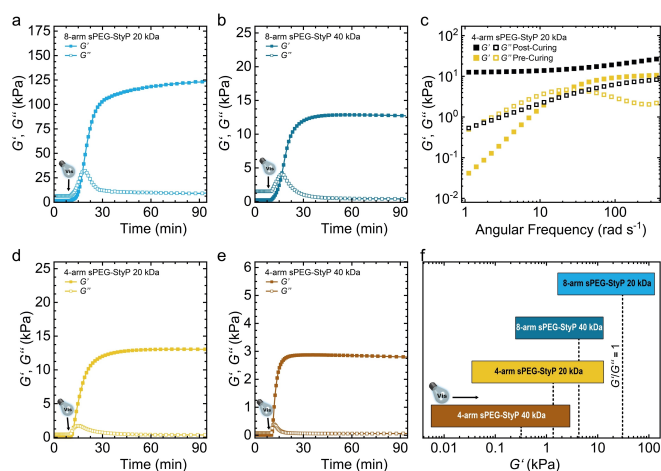
Conclusion

We introduce a molecular chaperone approach to facilitate the photochemical operation and structural ordering of bulky and hydrophobic photoswitches with red-shifted activation wavelength in water. Our strategy not only allows to increase the rate of the photochemical reaction and the extent of it on a molecular scale, but critically on a materials scale, i.e., for hydrogels. The approach enables preventing phase segregation and pre-orders star-shaped hydrogel prepolymers into quasi-ideal network as seen by the near perfect Maxwell behavior. This strikingly contrasts the poorly soluble and phase-segregating systems without the γ-CD chaperone. The ideal network behavior further allowed us to obtain a deeper understanding of the kinetics and thermodynamics of the complex supramolecular gels by temperature-dependent characterization of the network parameters. Based on the determined activation energies for

Figure 6. Photodimerization of supramolecular dynamic to covalent static networks. (a, b, d, e) Rheological profiles during visible light ($\lambda = 430$ nm, ca. $20 \, \text{mW} \, \text{cm}^{-2}$, $\omega = 1 \, \text{rad} \, \text{s}^{-1}$, $\gamma = 1\%$) induced crosslinking of four different sPEG-StyPs at c* in presence of equimolar amount of γ-CD in relation to StyP. Light bulbs highlight the start of irradiation at $t = 10$ min. In all systems the transition from visco-elastic liquid to elastic solid ($G' = G''$) occurs within 5 min and reaches a plateau of the storage modulus (G') after 20 min. (c) Frequency sweeps of 4-arm sPEG-StyP 20 kDa/γ-CD show transition from visco-elastic liquid to elastic solid state before and after curing, respectively ($\gamma = 1\%$). (f) The final moduli scale with the crosslinking density which correlates with the topology of the sPEGs. G'/G'' crossovers are indicated with dashed lines.

dissociation and association, the network formation based on the inclusion complex is both thermodynamically and kinetically favored.

Irradiation of the dynamic networks with visible light at 430 nm was used to trigger the photodimerization leading to a crosslinked network with quasi-ideal topology within 20 min. The final moduli scale with the crosslinking density, which correlates with the architecture of the sPEG-StyP building blocks. This is especially interesting as the properties of the networks become programmable and are no longer dependent on kinetic effects of dispersing a phase-segregated sPEG-StyP suspension in water prior photocrosslinking, which would be the case in absence of γ-CD.

Our supramolecular complexation approach appears overall promising for ideal structure formation for gel materials based on red-shifted chromophores in general and would enable a more effective materials preparation. We believe that similar approaches should be applicable for other red-shifted photoactive chromophores, as StyP is after all already a very bulky photoactive molecule. Our system can for instance serve as a more reliable platform to study material-cell interactions, such as mechanosensing, which critically depends on reliable material preparation protocols.

Supporting Information

The authors have cited additional references within the Supporting Information.[18]

Acknowledgements

Conflict of Interest

The authors declare no conflict of interest.

Data Availability Statement

The data that support the findings of this study are available from the corresponding author upon reasonable request.

Keywords: red-shifted photocycloaddition · cyclodextrin · model network · StarPEG · hydrogel

[1] a) E. R. Ruskowitz, C. A. DeForest, *Nat. Rev. Mater.* **2018**, *3*, 17087; b) L. Li, J. M. Scheiger, P. A. Levkin, *Adv. Mater.* **2019**, *31*, 1807333-NA; c) P. Lu, D. Ahn, R. Yunis, L. Delafresnaye, N. Corrigan, C. Boyer, C. Barner-Kowollik, Z. A. Page, *Matter* **2021**, *4*, 2172–2229; d) J. Cao, D. Zhang, Y. Zhou, Q. Zhang, S. Wu, *Macromol. Rapid Commun.* **2022**, *43*, e2100703; e) K. Peng, L. Zheng, T. Zhou, C. Zhang, H. Li, *Acta Biomater.* **2022**, *137*, 20–43.

[2] a) I. M. Irshadeen, S. L. Walden, M. Wegener, V. X. Truong, H. Frisch, J. P. Blinco, C. Barner-Kowollik, *J. Am. Chem. Soc.* **2021**, *143*, 21113–21126; b) S. L. Walden, L. L. Rodrigues, J. Alves, J. P. Blinco, V. X. Truong, C. Barner-Kowollik, *Nat. Commun.* **2022**, *13*, 2943; c) P. W. Kamm, L. L. Rodrigues, S. L. Walden, J. P. Blinco, A. N. Unterreiner, C. Barner-Kowollik, *Chem. Sci.* **2022**, *13*, 531–535; d) T. N. Eren, F. Feist, K. Ehrmann, C. Barner-Kowollik, *Angew. Chem. Int. Ed.* **2023**, e202307535; e) S. L. Walden, J. A. Carroll, A. N. Unterreiner, C. Barner-Kowollik, *Adv. Sci.* **2023**, 2306014.

[3] a) K. A. Gunay, T. L. Ceccato, J. S. Silver, K. L. Bannister, O. J. Bednarski, L. A. Leinwand, K. S. Anseth, *Angew. Chem. Int. Ed.* **2019**, *58*, 9912–9916; b) M. C. Paderes, M. Jeffrey Diaz, C. A. Pagtalunan, D. A. Bruzon, G. A. Tapang, *Chem. Asian J.* **2022**, *17*, e202200193.

[4] a) S. R. Trenor, A. R. Shultz, B. J. Love, T. E. Long, *Chem. Rev.* **2004**, *104*, 3059–3077; b) D. Lu, M. Zhu, S. Wu, Q. Lian, W. Wang, D. Adlam, J. A. Hoyland, B. R. Saunders, *Adv. Funct. Mater.* **2020**, *30*.

[5] a) K. Miyamoto, M. Sasaki, Y. Minamisawa, Y. Kurahashi, H. Kano, S. Ishikawa, *J. Biomed. Mater. Res. Part A* **2004**, *70*, 550–559; b) S. Yano, T. Iwase, N. Teramoto, T. Shimasaki, M. Shibata, *Carbohydr. Polym.* **2018**, *184*, 418–426.

[6] a) K. Min, S. Kim, S. Kim, *Proc. Natl. Acad. Sci. USA* **2017**, *114*, 6185–6190; b) M. Osaki, K. Ito, Y. Ikemoto, H. Yamaguchi, Y. Chujo, A. Harada, K. Tanaka, Y. Takashima, *Eur. Polym. J.* **2020**, *134*.

[7] E. R. Ruskowitz, C. A. DeForest, *ACS Biomater. Sci. Eng.* **2019**, *5*, 2111–2116.

[8] a) V. X. Truong, F. Li, J. S. Forsythe, *ACS Macro Lett.* **2017**, *6*, 657–662; b) V. X. Truong, F. Li, F. Ercole, J. S. Forsythe, *ACS Macro Lett.* **2018**, *7*, 464–469; c) D. E. Marschner, H. Frisch, J. T. Offenloch, B. T. Tuten, C. R. Becer, A. Walther, A. S. Goldmann, P. Tzvetkova, C. Barner-Kowollik, *Macromolecules* **2018**, *51*, 3802–3807; d) K. Murayama, Y. Yamano, H. Asanuma, *J. Am. Chem. Soc.* **2019**, *141*, 9485–9489; e) K. Kalayci, H. Frisch, C. Barner-Kowollik, V. X. Truong, *Adv. Funct. Mater.* **2020**, *30*; f) K. Kalayci, H. Frisch, V. X. Truong, C. Barner-Kowollik, *Nat. Commun.* **2020**, *11*, 4193; g) S. Ludwanowski, D. Hoenders, K. Kalayci, H. Frisch, C. Barner-Kowollik, A. Walther, *Chem. Commun.* **2021**, *57*, 805–808; h) D. Kodura, L. L. Rodrigues, S. L. Walden, A. S. Goldmann, H. Frisch, C. Barner-Kowollik, *J. Am. Chem. Soc.* **2022**, *144*, 6343–6348; i) V. X. Truong, J. Bachmann, A. N. Unterreiner, J. P. Blinco, C. Barner-Kowollik, *Angew. Chem. Int. Ed.* **2022**, *61*, e202113076.

[9] a) T. L. Rapp, C. A. DeForest, *Adv. Healthcare Mater.* **2020**, *9*, e1901553; b) V. X. Truong, C. Barner-Kowollik, *Trends Chem.* **2022**, *4*, 291–304.

[10] a) T. Tamaki, T. Kokubu, *J. Inclusion Phenom.* **1984**, *2*, 815–822; b) J. N. Moorthy, K. Venkatesan, R. G. Weiss, *J. Org. Chem.* **1992**, *57*, 3292–3297; c) S. Tamagaki, K. Fukuda, H. Maeda, N. Mimura, W. Tagaki, *J. Chem. Soc. Perkin Trans. 2* **1995**, 389–393; d) W. Herrmann, S. Wehrle, G. Wenz, *Chem. Commun.* **1997**, 1709–1710; e) K. S. Rao, S. M. Hubig, J. N. Moorthy, J. K. Kochi, *J. Org. Chem.* **1999**, *64*, 8098–8104; f) T. J. Brett, J. M. Alexander, J. J. Stezowski, *J. Chem. Soc. Perkin Trans. 2* **2000**, 1095–1103; g) C. Yang, Y. Inoue, *Chem.*

Soc. Rev. **2014**, *43*, 4123–4143; h) B. Bibal, C. Mongin, D. M. Bassani, *Chem. Soc. Rev.* **2014**, *43*, 4179–4198; i) X. Zhang, X. Ma, K. Wang, S. Lin, S. Zhu, Y. Dai, F. Xia, *Macromol. Rapid Commun.* **2018**, *39*, e1800142.

[11] a) Q. Zhang, D. H. Qu, X. Ma, H. Tian, *Chem. Commun.* **2013**, *49*, 9800–9802; b) F. Biedermann, I. Ross, O. A. Scherman, *Polym. Chem.* **2014**, *5*, 5375; c) G. Liu, Q. Yuan, G. Hollett, W. Zhao, Y. Kang, J. Wu, *Polym. Chem.* **2018**, *9*, 3436–3449; d) L. Zou, M. J. Webber, *Chem. Commun.* **2019**, *55*, 9931–9934; e) A. Tabet, R. A. Forster, C. C. Parkins, G. Wu, O. A. Scherman, *Polym. Chem.* **2019**, *10*, 467–472; f) Z. Hou, W. M. Nau, R. Hoogenboom, *Polym. Chem.* **2021**, *12*, 307–315.

[12] a) Y. Zhang, D. Yang, J. Han, J. Zhou, Q. Jin, M. Liu, P. Duan, *Langmuir* **2018**, *34*, 5821–5830; b) Y. Ohishi, M. Inouye, *Tetrahedron Lett.* **2019**, *60*; c) Q. Wang, Q. Zhang, Q. W. Zhang, X. Li, C. X. Zhao, T. Y. Xu, D. H. Qu, H. Tian, *Nat. Commun.* **2020**, *11*, 158.

[13] W. Liu, X. Gong, Y. Zhu, J. Wang, T. Ngai, C. Wu, *Macromolecules* **2019**, *52*, 8956–8966.

[14] a) M. Asai, T. Katashima, U.-i. Chung, T. Sakai, M. Shibayama, *Macromolecules* **2013**, *46*, 9772–9781; b) G. A. Parada, X. Zhao, *Soft Matter* **2018**, *14*, 5186–5196.

[15] A. S. Braegelman, R. C. Ollier, B. Su, C. J. Addonizio, L. Zou, S. L. Cole, M. J. Webber, *ACS Appl. Bio. Mater.* **2022**.

[16] a) T. Sakai, T. Matsunaga, Y. Yamamoto, C. Ito, R. Yoshida, S. Suzuki, N. Sasaki, M. Shibayama, U.-i. Chung, *Macromolecules* **2008**, *41*, 5379–5384; b) T. Matsunaga, T. Sakai, Y. Akagi, U.-i. Chung, M. Shibayama, *Macromolecules* **2009**, *42*, 1344–1351; c) A. Sugimura, M. Asai, T. Matsunaga, Y. Akagi, T. Sakai, H. Noguchi, M. Shibayama, *Polym. J.* **2012**, *45*, 300–306; d) T. Hiroi, M. Ohl, T. Sakai, M. Shibayama, *Macromolecules* **2014**, *47*, 763–770; e) K. Nishi, H. Asai, K. Fujii, Y.-S. Han, T.-H. Kim, T. Sakai, M. Shibayama, *Macromolecules* **2014**, *47*, 1801–1809; f) T. Sakai, *Polym. J.* **2014**, *46*, 517–523; g) T. Sakai, *Physics of Polymer Gels* **2020**.

[17] a) X. Wei, W. Wu, R. Matsushita, Z. Yan, D. Zhou, J. J. Chruma, M. Nishijima, G. Fukuhara, T. Mori, Y. Inoue, C. Yang, *J. Am. Chem. Soc.* **2018**, *140*, 3959–3974; b) B. Marco-Dufort, R. Iten, M. W. Tibbitt, *J. Am. Chem. Soc.* **2020**, *142*, 15371–15385.

[18] T. Doi, H. Kawai, K. Murayama, H. Kashida, H. Asanuma, *Chem. Eur. J.* **2016**, *22*, 10533–10538.